Materials Engineering and Development for Coal Fired MHD Power Generators

L. M. RARING

This paper attempts to describe the unique stresses imposed on MHD generator materials. This is done by reviewing experimental test histories of two generator designs representing extremes in operating conditions and materials selection. Related experimental work, bearing on the importance of coal-ash slag properties to design functions, is also reviewed. This latter is particularly critical to U.S. MHD development goals. The range of engineering conditions and materials attending the tests described in this review suggests a breadth of design choice which is probably less real than apparent. Engineering development, currently in progress and planned, is directed towards quantitative determination of specific design and material influences on generator performance and durability. Material requirements are closely interrelated with thermal, electrical, and geometric design conditions, as this review will show. Finally, MHD test experience summarized here affirms the necessity for close engineering design and test discipline in the development of materials for power machinery applications.

A. INTRODUCTION

THE strong national incentive to produce electricity directly from coal underscores magnetohydrodynamic (MHD) development. Independent studies have predicted coal-to-busbar efficiencies of 48 to 50 pct or more for combined open-cycle MHD-steam systems.[1] These same studies estimated cost-of-electricity for a number of advanced energy conversion systems based on fossil fuel: The coal-fired MHD-steam combination was lowest. Moreover, this MHD system could use high sulfur coal with no additional stack gas clean-up because sulfur is removed in the MHD power cycle.

The first exploratory work on commercial MHD power was undertaken by a group of Northeast utilities in the early sixties. The Government, through the Office of Coal Research (OCR) of the Department of Interior, initiated analytical and experimental studies, directed toward commercial MHD power, in 1966. A separate Division of MHD was formed by the Energy Research and Development Administration (ERDA) in September 1975, as commercial potentialities became increasingly apparent.

The Department of Energy MHD program divides typically into three progressive phases. First, Engineering feasibility must be convincingly demonstrated by successful operation of an integrated subscale power system under design conditions which would be expected in central station duty. The second phase demonstrates commercial feasibility through the successful operation of a larger scale, fully integrated MHD-steam combined cycle pilot plant. The third and final phase is directed toward commercial operation of a large MHD-steam combined cycle power station.[2]

The program is currently in the first phase. Development efforts are aimed toward the design of engineering demonstration generator systems of 50 MW (thermal) capacity. The Electric Power Research Institute (EPRI) is supporting complementary development work.[3]

In considering materials for MHD power, two related observations are noteworthy: a) materials are crucial to commercial success; and b) material stresses, particularly in the generator, are unique. MHD power conversion has no direct precursor in established power conversion technology. No rotating parts are imposed between the fuel combustor and the power take-off. MHD generators place greatest premium on maximum resistance to elevated temperature electrochemical stresses rather than mechanical stresses. The transference of elevated temperature materials problems from the mechanical to the electrochemical regime is more understandable when one recognizes MHD as an electromagnetic turbine. Heat fluxes are also considerably higher than in conventional power conversion cycles.

After a brief description of MHD design principles, the paper will attempt to describe the generator electrochemical and thermal stress environment. A summary of the performance of some of the more prominently tested generator materials will then be presented. Material requirements for the combustor, air heater, boiler, and other plant components, while formidable, do not present uniquely new challenges as does the generator and will not be discussed in this paper. The paper will conclude with a brief summary of test results in relation to design criteria.

B. DESIGN PRINCIPLES

MHD power generation is based on the direct conversion of heat to electrical energy by expanding a heated, electrically conducting fluid through a magnetic field. Thus, the essential difference between an MHD generator and a conventional turbine-driven generator is that in the MHD generator the rotor is replaced by a high velocity, ionized working fluid. The interaction of this high temperature conducting fluid with a strong, transverse magnetic field induces an electromagnetic field approximately proportional to the product of the magnetic field and the velocity. Spatial relationship is analogous to conventional gen-

L. M. RARING is Assistant Director, Technology(Acting), Division of Magnetohydrodynamics, Department of Energy, Washington, DC 20545.

This paper is based on a presentation made at a symposium on "Materials Requirements for Unconventional Energy Systems" held at the Niagara Falls meeting of The Metallurgical Society of AIME, September 22, 1976, under the sponsorship of Non-Ferrous Metals and Ferrous Metals Committees.

ISSN 0360-2133/78/0210-0161$00.75/0

erator operation as indicated schematically in Fig. 1.

The duct walls at right angles to the magnetic field are nonconducting. Electrodes are imbedded in the two walls parallel to the magnetic field. These electrodes collect the DC current produced by the induced EMF.

Current density, J, induced by the reaction of the flowing fluid with the magnetic field is expressed by:

$$J = \sigma UB + \sigma E = \sigma(E - UB)$$

where σ = conductivity (mho/meter); E = electric field (volt/meter); B = magnetic flux density (Weber/Meter^2); U = gas velocity (meter/second).

The most influential parameters in the determination of power density in the channel are gas conductivity, gas velocity, and magnetic flux density. Potassium seeding is employed to improve conductivity.

The MHD topping unit in a coal-fired, base load combined cycle power plant would be expected to convert 15 pct or more of the available enthalpy to DC power. This combined with a 35 or 40 pct conversion of the remaining thermal energy of the gas stream in the steam bottoming plant would deliver an overall efficiency of nearly 50 pct. Improvements in the MHD cycle, which may be within reach,[1] could increase overall efficiencies to 55 or 60 pct.

Regenerative heat exchangers are required to preheat the combustion air supply to at least 1475 K in order to achieve combustion temperatures of up to 2875 K. The skeletal lay-out shown in Fig. 2 is representative of a probable arrangement of major components in an integrated combined-cycle plant.[2]

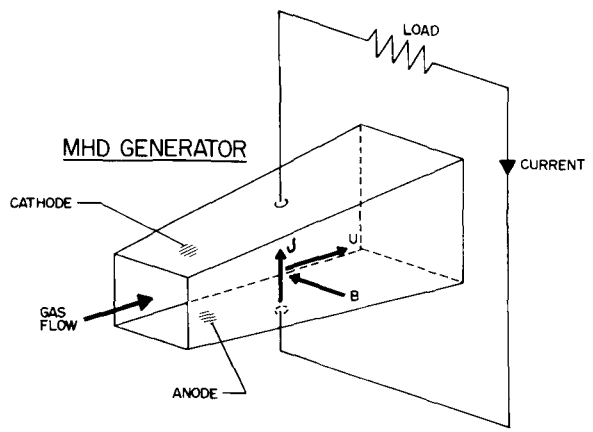

Fig. 1—Spatial relationship of magnetic flux density (B), plasma flow velocity (U), and electric current density (J).

C. DESIGN CONSIDERATIONS

We will first consider the nature of the chemical, thermal, and electromagnetic stresses which prevail at various critical surface and subsurface regions of the generator interior walls. From the viewpoint of the materials engineer, these stresses dictate the essential design requirements for generator materials. No attempt will be made to explain electromagnetic phenomena. Reference 4 is recommended for study of electrodynamic and fluidynamic theory and related engineering requirements.

As noted previously, the critical function of the electrodes is to collect electric charges from the plasma. This is the first link in transporting current to the external load. Internal current flows from anodes, across the core to cathodes, and thence through the load circuit back to anodes. In passage across the core, the current transverses boundary layers (including the slag coating) on both electrodes. High conductivity is important to avoid excessive Joule losses.

The Hall Effect exerts a strong influence on electrode design because it causes the current to flow at an angle of about 60 deg with the local electric field. Electrodes must be segmented to minimize the interelectrode voltage differentials which result. This requires that each electrode be electrically isolated from its upstream and downstream neighbor. The interelectrode insulator, which serves this purpose, must be capable of withstanding potential differences of up to 70 or 80 V. In some electrical designs, transverse current leakages must be blocked also between active sidewall elements at different potential levels.

Under generating conditions, MHD electrodes function somewhat similarly to those of a common battery. Electrochemical influences are analogous even though heat transfer rates and thermochemical and electrodynamic conditions are vastly different. The critical importance of interelectrode insulation adds an additional dimension.

Electrochemical effects on electrodes result principally from concentrations of positive ions at the cathode and negative ions at the anode. Seed flow, coal chemistry, slag carry-over, and combustion conditions all influence the species and concentrations at the electrode (and adjacent insulator boundary). The most aggressive species, as will be illustrated later, are oxygen at the anode (for metallic systems) and potassium, calcium, and iron at the cathode. Under ordinary thermal conditions, these environments could be readily dealt with, but under the special high tempera-

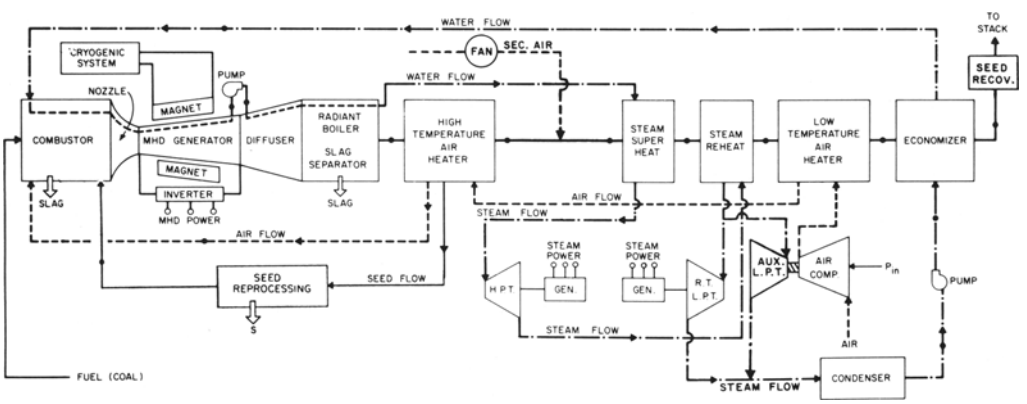

Fig. 2—Simplified schematic of directly fired air preheater system configuration.

ture and electrodynamic conditions which exist at the channel wall, the problem becomes more complex.

Thermal design impinges strongly on both electrodynamic and electrochemical effects. Higher temperatures minimize Joule losses in the boundary layer (slag and plasma) but accelerate chemical and structural degradation (electrically driven or otherwise). Lower temperature electrodes show opposite effects, *e.g.*, reduced chemical attack but less favorable current transfer. A design dichotomy thus exists between favorable current transfer, on one hand, and wall materials durability on the other.

Another electrodynamic effect which must be considered is that the Hall Effect tends to crowd the current toward the leading edge of the anode and the trailing edge of the cathode. This means that a nominal 1 A/cm^2 maximum current density may locally go much higher, exacerbating chemical and/or structural degradation of wall materials.

[It should be emphasized that regardless of the special thermal design of the electrode wall, the slag surface above the electrode constitutes the true "electrode" surface. When we talk of metal or ceramic electrode temperatures, we are really dealing with thermal, electrochemical, and physical phenomena at the interface of the "slag electrode" and the support structure.]

This has been a very cursory view of the design stresses exerted on channel walls and the range of conditions which prevail. References 5 and 6 are recommended for more detailed understanding.

D. TEST EXPERIENCE

This section will review some of the more significant results of material tests conducted in experimental generators or in MHD simulator tests. No attempt will be made to discuss the results of numerous studies which have been reported on slag physical and chemical properties[7-11] or generator material laboratory tests and development.[12-15]

The most significant materials test experience falls into three classes: a) tests in experimental open-cycle MHD generators burning clean fuel; b) tests in experimental open-cycle MHD generators burning coal or simulating coal combustion to provide a slag coating on the walls of the channel; and c) laboratory tests which partially simulate MHD stresses.

United States interest in MHD power is, of course, based upon coal-fueled operation–this dictates a finite carry-over of volatilized or liquid coal-ash from the combustor into the generator channel. Two approaches are being taken. In one, all of the slag produced by combustion of the coal is led into the channel. Liquid slag containing seed flows down the channel and diffuser walls from where, in the conceptual plant scheme of Fig. 2, it would flow into the radiant boiler. Most of this slag would eventually be tapped from the gas stream, probably at the exit of the regenerative heater. The second approach is to tap-off most of the liquid slag in the combustor, before adding the seed. The remaining slag enters the channel at a lower fraction of the total mass flow, but sufficient to build up and maintain a continuous coating on the channel walls. Slag and seed removal are accomplished in the downstream gas path, where thermodynamic conditions are most favorable.

MHD development under clean fuel conditions is being pursued in the USSR. Despite the absence of coal on the channel walls, tests under these conditions can provide useful data on electrode and insulator materials, especially with regard to electrothermal stability, potassium resistance, and current lead-out design requirements. Material tests in generators operating in the "slagging mode" are being conducted by several U.S. organizations.[16-18]

For a true perspective on the design stresses which generator materials must endure, it is useful to review test experience under both "clean" and "dirty" (slagging) conditions.

D.1. Clean Fuel Test

"Clean" fuel tests were conducted in the USSR U-02 test facility, a small-scale model of a complete MHD plant.[19] Thermal capacity is approximately 5 MW and mass flow close to 1 kg/s. As part of the U.S.-USSR Cooperative Program on MHD, a series of tests is being conducted jointly in the facilities of both countries to evaluate various electrode design features. The test results discussed here were obtained between September 25 and October 1, 1975, in the USSR U-02 facility.[20] The test assembly consisted of a rectangular Faraday generator section comprising electrode walls on the top and bottom and insulator side walls at the sides. Internal dimensions were 26.0 cm high by 64.0 cm wide for a constant cross-sectional flow area of 1664 cm^2. Twenty transverse rectangular electrodes were equally spaced along the electrode walls. Electrode dimensions, in relation to the channel axis, were 12 mm long, 62 mm wide, and 6 mm thick. The electrodes were separated by 12 mm of high purity MgO of approximately 85 pct theoretical density. Electrode pairs were connected to separate loads with interelectrode potentials estimated at 15 V. The channel insulating side walls consisted of hexagonal MgO blocks brazed to a copper base. The electrode walls were designed and fabricated in the U.S., while the insulating walls were provided by the USSR.

The electrode walls consisted of five separate segments, each with four electrodes of the same material, *viz*:

Group	Nominal Composition, mol pct
I	88 ZrO_2:12 Y_2O_3
II	82 ZrO_2:18 CeO_2
III	50 ZrO_2:50 CeO_2
IV	25 ZrO_2:75 CeO_2
V	20 ZrO_2:78 CeO_2:2 Ta_2O_5

Electrical lead-outs were provided by metallizing the back side of each electrode with a thin coating of platinum to which a platinum screen was attached. This was accomplished by firing several successive coatings of platinum paste. The screen was incorporated with the final paste applications. External connection was made by means of a 0.51 mm platinum wire welded to the screen. The proprietary magnesia interelectrode insulating blocks were fabricated by hot pressing to about 85 pct TD. The hot pressed blocks, 152 mm × 152 mm × 36.5 mm, were ground to final

shape. A commercial zirconia phosphate cement was used between the electrode and insulator. In other wall areas, away from the electrodes, a calcia-zirconia cement was used to seal interface joints.

After a low temperature (525 K) preheat, the system was fired at maximum turn-down ratio with natural gas (97 pct methane, 2 pct ethane, 1 pct inerts). Heating rate as measured by thermocouples mounted in the electrode module averaged 50 K/min. After 30 min, combustion conditions were gradually brought up to operating levels. Baseline plasma conditions were as follows:

Oxygen enrichment: 40 mol pct;
Plasma temperature: 2300°C;
Mass flow: 0.75 Kg/s;
Static pressure: 0.83 atm;
Potassium seed: 1.0 wt pct;
Average velocity: 450 m/s; and
Conductivity: 10 mhos/m.

Seeding was accomplished by injecting a 50 pct K_2CO_3-50 pct H_2O mixture into the combustor. Magnetic field strength was 1.7 T. Nominal heat fluxes in the electrode walls at the entrance and exit were 30 W/cm^2 and 18 W/cm^2, respectively.

The test was designed to obtain temperatures in the fourth anode between 1975 K and 2050 K.

The test profile required, first, an 18 h run, with no seed, to establish and stabilize the desired thermal conditions. The next 6 h were used to determine the electrical characteristics of the test module under power conditions. Power testing was continued for 94 h to evaluate durability. The test was then terminated in 9 h, allowing for cool down and disassembly.

Temperature measurements of the first group of electrodes showed 1985 K at the surface (optical pyrometer) and 1455 K 3 mm below the surface. Three short-duration plasma temperature excursions occurred during test. These were reflected by temperature rises of 360, 425, and 140 K at the subsurface thermocouple location. Duration of these excursions did not exceed 5 min.

Average thermal fluxes during test were 23 W/cm^2 on the cathode wall and 22.9 W/cm^2 on the anodes. Calculations of surface temperatures from thermal flux data and thermocouple readings suggested that first group cathode temperatures exceeded first group anode temperatures by 50 to 100 K. Maximum surface temperatures were estimated to be between 2025 and 2075 K. Temperatures gradually decreased in the downstream direction. The fifth cathode module surface temperature was estimated as between 1925 and 1975 K. These estimates are again based upon subsurface temperature readings and heat flux data. During the 94 h life test, the electrodes of each group were operated at four current density levels, *viz*: 0 A/cm^2, 0.24 to 0.33 A/cm^2, 0.5 to 0.7 A/cm^2, and 1.2 A/cm^2. These conditions were obtained through controlled external loading.

Post-Test Analyses.[20] Visual inspection following tear-down revealed the following:

a) Penetration of the interface joints connecting the test section with the nozzle and diffuser by foreign material, presumably potassium compound.

b) Moderate degradation of electrodes by erosion or corrosion and cracking, more pronounced on cathode walls.

c) Electrode swelling and spalling, particularly noticeable on cathodes, on ZrO_2-CeO_2 materials, and on electrodes carrying higher current densities.

d) Interelectrode MgO insulators erosion to depths of 1 to 3 mm, particularly on cathode wall. Longitudinal cracking observed near the centers of the insulators on both electrode walls. Damage most severe on insulators adjacent to electrodes carrying higher currents.

Three longitudinal sections were cut from both electrode walls. Figures 3 and 4 are photographs of two of these sections. Post-test laboratory samples were prepared from these sections for detailed metallographic, SEM, electron microprobe, X-ray diffraction (XRD), radiographic, and chemical analyses. In addition, electrical conductivity measurements were made on specimens taken from several anodes. Significant findings based on these extensive investigations are summarized below.

a) Maximum potassium concentrations were identified in regions adjacent to the interface between the electrode base and the MgO insulator cup. Lesser concentrations were noted in side wall interface regions near the bottom of the electrode. Potassium

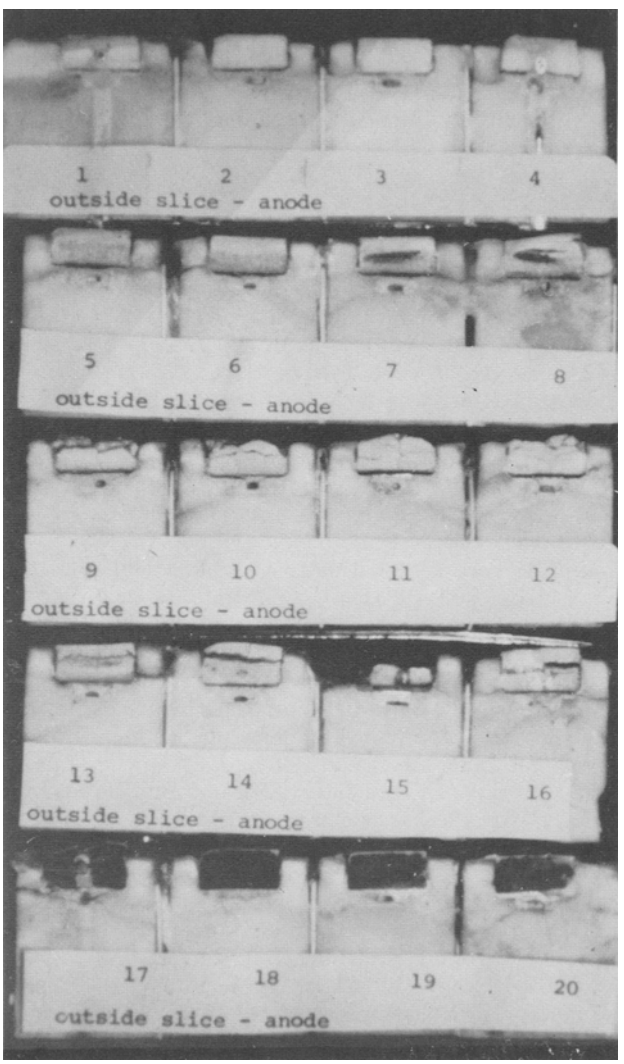

Fig. 3—Anode slices, magnification 0.74 times.

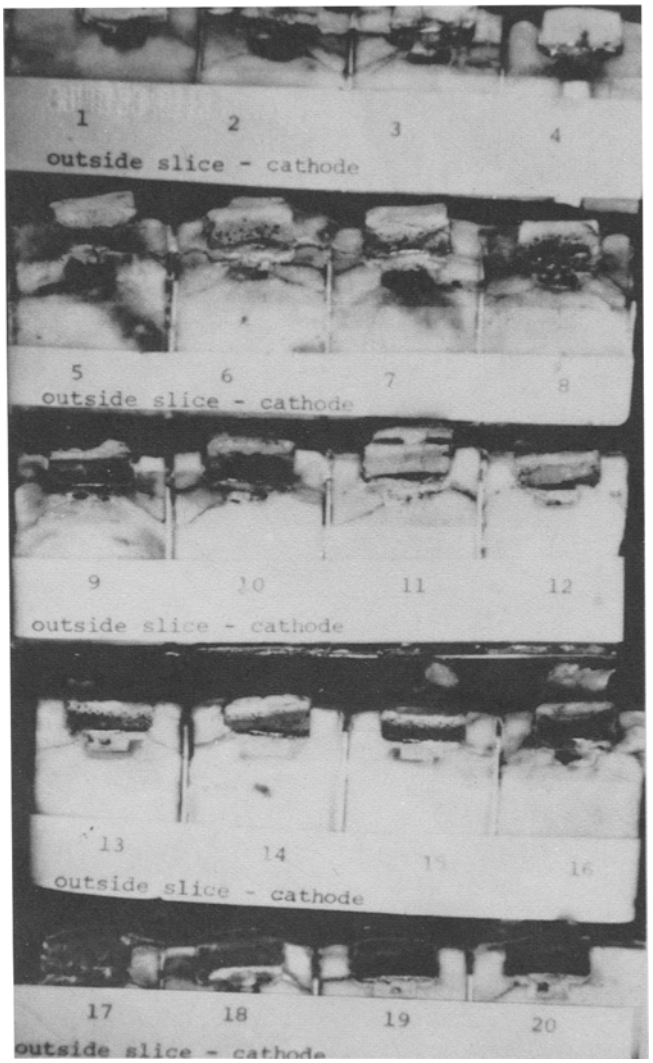

Fig. 4—Cathode slices, magnification 0.74 times.

concentrations decreased to negligible levels in interface regions closer to the plasma surface. This selective concentration of potassium strongly suggests: 1) gaseous transport of K_2CO_3 through the relatively porous zirconia phosphate cement between the electrode and MgO, and 2) condensation of K_2CO_3 in the cooler (975 K to 1575 K) regions at the base of the electrodes and below.

b) While the zirconia phosphate cement interface was probably the principle path of K_2CO_3 penetration, transport is believed to have been further facilitated by porosity in the MgO insulator, phase changes in the insulator and certain electrodes, and cracks in the MgO insulator. Evidence for these hypotheses are: 1) significant concentrations of K in the small grained, porous areas surrounding larger grains in the MgO structure, 2) XRD evidence of phase changes in certain electrodes and MgO insulators concomitant with potassium deposits, and 3) presence of potassium in cracks which originated at the corner between the side wall and base of the MgO cup.

c) The effects described in (a) and (b), above, were much more pronounced on the cathode wall than on the anode wall. Considering the cathode wall only, the ZrO_2-CeO_2 electrodes were most noticeably affected. Electrically loaded electrode pairs were affected more than those which did not carry an electric current.

d) The degree of swelling and fragmentation of electrodes (*i.e.*, protrusion above the original wall surface) was related qualitatively to potassium concentrations in the subsurface insulator-electrode interface regions. Thus, cathodes were much more affected than anodes; the equimolar ZrO_2-CeO_2 cathode showed the most severe damage, and electrical loading was again associated with intensified damage.

e) It is hypothesized that swelling and fragmentation of electrodes occurred with hydration of the K_2CO_3 deposits during cool down. The 40 to 60 pct volume expansion accompanying hydration would be expected to produce destructive mechanical stresses. Metallographic evidence sustains this explanation. Moreover, the extensive XRD evidence of phase transformations, especially in the ZrO_2-CeO_2 electrodes, implies residual stress intensification further contributing to mechanical damage.

The preceding summary of post-test analyses of the U-02 electrode walls emphasizes information and observations of most direct materials engineering and design concern. Reference 20 provides a more extended summary. The following paragraphs describe additional observations of importance to materials engineering concerns.

Insulators. The MgO insulators had recrystallized to depths of as much as 0.4 cm. Insulator regions adjacent to the upstream side of the electrode exhibited greater degradation and structural change than regions adjacent to the downstream side. This was more pronounced on the anode wall than the cathode. Cracking of MgO insulators originated at the corner of machined recesses. These cracks did not vary noticeably with location of the insulator. Potassium was present in all these cracks.

On the cathode side, potassium penetrated the insulator and ZrO_2 cement materials beyond the thickness of the electrode insert, whereas on the anode side, penetration beyond the body of the electrode was negligible. Again, on the cathode side, greatest depths of potassium penetration corresponded to highest current densities.

Electrodes. The most noticeable effects on ZrO_2-CeO_2 cathode structures were phase transitions and/or potassium reaction. Detailed discussion of the XRD data is beyond the scope of this review, but it should be noted that substantial evidence was developed to postulate the *in situ* reduction (at test temperature) and reoxidation (during cooldown) of the ZrO_2-CeO_2 material. Loss of CeO_2 by vaporization was also established.

The $88ZrO_2$-$12Y_2O_3$ cathode appeared to have recrystallized to a depth of less than 1 mm. This thin surface zone buckled and separated from the substrate. Monoclinic (destabilized) zirconia as well as a cubic zirconia solid solution, with a cubic cell parameter smaller than that for the virgin 88-12 structure, were detected in some regions at the bottom of the electrode.

Lead-Outs. Lead-out failures, which occurred on six electrode pairs, are ascribed to melting of the 0.51 mm platinum wire. There was no indication that chemical attack had contributed to these failures. A more probable explanation, based upon experimental

observation, is that intense Joule heating was responsible, induced perhaps by a locally constricted cross-section (mechanical defect) combined with impaired heat transfer (poor contact with the ZrO_2 cement).

This test revealed material and design weaknesses (as it was intended) in the first U.S. electrode modules tested in the U-02 facility. Foremost, it clearly highlights the importance of preventing transport of gaseous KCO_3 into the cooler, internal regions of either the electrode or insulator structure. In this design, access to the substrate regions are apparently afforded principally by the ZrO_2 phosphate bond between the electrode and MgO cup.

The test also provides useful information on certain ceramic electrode materials behavior within known operating boundary conditions. It is reasonably certain, for example, that the ZrO_2-CeO_2 materials are unsuited to cathode applications under the thermal design conditions which existed in this test. The ZrO_2-Y_2O_3 cathode also exhibited structural instabilities under these test conditions.

It is not clear whether, in the absence of potassium penetration, these materials would be suited to long-life anode duty. Indications of structural instabilities would suggest not.

MgO insulator stability was probably severely compromised by exposure to K_2CO_3 which initially gained access mainly through the cement. Nevertheless, the presence of potassium in association with the fine grained regions of the MgO clearly points to the need for higher density materials or effective barriers.

XRD evidence of Al_2O_3 vapor transport points to the possible unsuitability of this material in high temperature, upstream wall applications.

The lead-out problem disclosed in this test indicates the necessity for sturdier design of this important interface. It should be noted that the major portion of physical damage to the cathode wall probably occurred during cool-down. Despite the obvious instabilities noted, shutdown was not forced and power operation could probably have been continued for some additional time.

Finally, it is not surprising to find potassium preferentially concentrated at the cathode wall in view of the electromotive forces which prevail in the channel. The electrode walls experience similar electrochemical conditions as are induced in electrolytic current transfer. Positive potassium ions would thus be attracted to the cathode wall and repelled at the anode wall. Increasing current density would intensify this electrolytic effect, as indicated qualitatively by the laboratory findings.

D.2. Simulated Coal-Fired Test

This test was conducted in a channel modeling experimental generator test rig, designated the Mark VI by the EVCO Everett Research Laboratory, Inc.[21] Essential elements of this test rig comprise an oil-fired combustor; the channel, including the inlet nozzle and diffuser; instrumentation and controls; and a 30,000 G water-cooled iron core magnet. The Mark VI-C diverging channel dimensions were: length: 2 m; average cross-section: 210 cm^2; exit to inlet area ratio: 3.3 to 1. The channel was operated supersonically to obtain maximum power levels available with

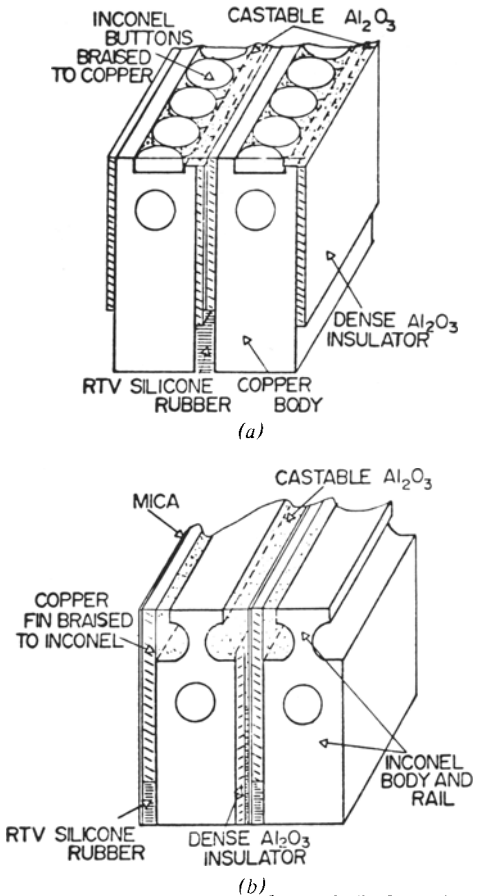

Fig. 5—(*a*) Button Wall Design. (*b*) Rail Wall Design. Plasma flow from left to right for cathodes, right to left for anodes.

a 3T field. This was necessary to ensure that MHD stress levels would most nearly simulate base load central station duty conditions. ("MHD stress" is used here to express the engineering design conditions which generator materials would be required to sustain in commercial service.)

The internal elements of the channel were mounted on fiberglass walls to form 108 segmented frames at an average angle of 45 deg relative to the channel axis. Each frame consisted of six electrically discontinuous Inconel elements. Two different thermal designs were tested. The first twenty electrodes used a new button design to provide an electrode surface temperature of approximately 815 K (Fig. 5(*a*)). The remaining electrodes represented a rail configuration, designed to achieve approximately 1370 K (Fig. 5(*b*)). The rail type electrodes had been used in previous tests. The buttons were new. Electrical connections of the channel frames are shown schematically in Fig. 6. The resultant loading of the generator is in a mixed mode where nominally 90 pct or more of the total power is delivered to a single main axial load (11 ohms for the Mark VI-C). Nominal test conditions are summarized in Table I.

Seed was injected as K_2CO_3, either dry or in an aqueous solution. Fly ash was injected at a rate to simulate 25 pct ash carryover from a coal combustor. Nominal fly ash composition and bulk slag product analysis is given in Table II.[22]

The test continued for 103 h. Power levels of 200 kw or more were achieved over the first 98 h. Total

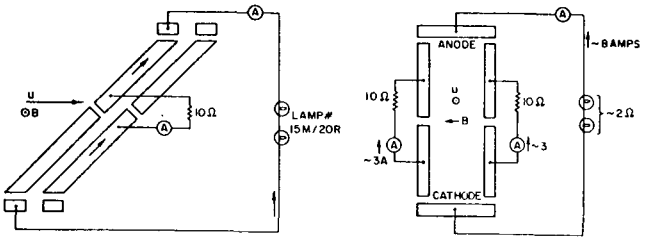

Fig. 6—Schematic of intraframe current controls, Mark VI-C channel.

power extraction was 20,500 kWh. Average power density was 5 MW/m^3 with a peak density of 12.5 MW/M^3. Maximum current density was 1 A/cm^2 with Hall voltages up to 1500 V/m. Inspection after tear-down revealed two water leaks, one at a defective weld in the inlet nozzle and the other in the front side wall power take-off element.

Post-Test Analyses. Post-test analyses were performed by the National Bureau of Standards.[22] Results of most significant design interest to the Materials Engineer are summarized in this section. The referenced Bureau of Standards paper provides considerable additional data.

The post-test analytical data differentiates between thermal and polarity effects, as indicated in the following summary of significant findings.

Considering, first, thermal effects: It is instructive to directly compare the performance of the 1370 K rail design with the 810 K button design on the anode walls. The rail anode wall had eroded away to very nearly a plane surface, as illustrated schematically in Fig. 7. The button anode wall had eroded far less. In effect, then, erosion of the rail anode brought this design closer to the thermal conditions (810 K) of the button design. Moreover, oscillograph traces of the integrated cooling water bulk temperature rise on the anode wall suggest that thermal equilibrium was established within the first forty test hours.

Table I. Test Conditions for the Mark VI-C

Total mass flow	2.5 kg/s
N/O	0.8
Seed concentration	0.8 pct wt (powder) 1.2 pct wt (aqueous)
Ash flow rate	0.25 pct total mass flow
Burner stagnation pressure	3.5 atm
Channel inlet mach number	~1
Estimated stagnation temperature	2800 K

Electrochemical sensitivity is clearly illuminated by comparison of the rail anode with adjacent rail side wall. Presumably, the major difference here is current density: the electrode wall collects most of the Faraday current. This comparison reveals that erosion had proceeded farther on the anodes than on adjacent side walls, which sustained considerably lower current densities. This points to electrochemical influences operating concurrently with the thermal effect.

Further evidence of electrochemical influences were afforded by XRD, SEM, and metallographic analyses, of side wall rails, to wit:

"Erosion appears to occur not only on the rail top, but around the rounded edges and toward the neck. The SEM micrographs indicate that there are essentially three zones near the slag interface. The innermost zone is Inconel. The intermediate zone is vesicular and consists of Inconel ridges and irregular cavities rich in chromium and iron. This suggests that the nickel is oxidizing preferentially. The outer zone has a granular microstructure and consist of nickel, chromium and iron. We suggest that this area represents an oxidized scale which ultimately spalls and dissolves in the slag. The mechanism for this degradation must be related to active oxidation of the metal by chemical reaction with oxygen and/or to electrochemical corrosion reactions. It is unclear, however, whether the corrosion observed for the sidewall anode rails is the dominant process leading to destruction of the anode wall, in general. If destructive oxidation dominates, one would expect to find metal oxide components of Inconel in the slag adjacent to the anode electrodes. We searched for these components in the anode slag

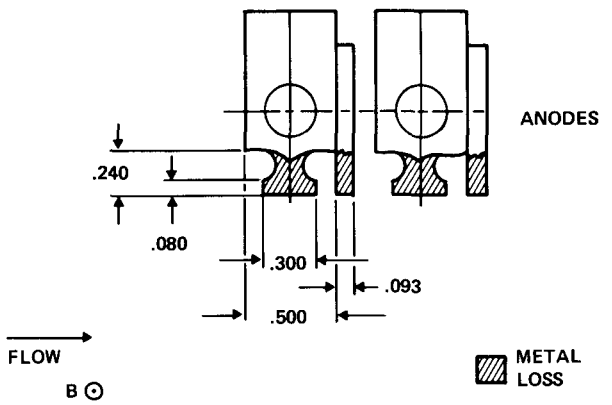

Fig. 7—Areas of electrode metal erosion after 150 power h.

Table II. Semiquantitative Spectrochemical Analysis of Bulk Slag Materials from Several Locations in the Generator System. Only Elements Significant to the Experiment are Listed (Wt Pct).

	Burner	Upstream Cathode	Upstream Anode	Cathode Exit	Anode Exit	Diffuser	Original Fly-Ash
Al	>13	>13	>13	>13	>13	>13	13.5*
Si	>13	>13	>13	>13	>13	>13	16.7*
K		>13	>13	>13	>13	>13	
Ca	1.5	2	1	1.5	1	1	4.08
Cr	0.05	<0.05	<0.05	0.15	0.15	0.05	
Ni	0.05	0.2	0.2	0.5	0.2	0.2	
Fe	>13	>13	5 to 10	5 to 10	5 to 10	>13	13
Cu	0.15	3	1.5	0.05	1.5	0.05	

*Wet chemical analysis.

but could not find significant amounts. However, if the slag is exchanged frequently, metal components would not be present in the newly formed slag. As the total mass ratio of metal removed to coal slag fed to the channel during the 100 h run is small, a dilution effect is operative. Previous analysis of AVCO cathode and anode slag under different conditions did show 1 to 5 wt pct of nickel in localized spots in the anode slag."[22]

These observations were made on the remnant rail sections of the anode side wall. The anode wall rails had eroded to an essentially plane surface, as previously noted.

Principle electrochemical influences are, however, most clearly exemplified by comparison of anode and cathode walls.

The most noticeable distress on the cathode wall is illustrated schematically by Fig. 8. This sketch identifies three zones in the space between the copper fin of the downstream rail electrode and the Inconel rail of the upstream electrode. In the sketch, the plasma flow is left (upstream) to right (downstream). The volume (labeled a, b, c) was initially filled with cast Al_2O_3. Detailed analyses of the "slag" material found in this space after test showed:

Area a–glassy, no crystalline phases containing K, although some K is present, presumably in solution.

Area b–contains crystalline orthorhombic $KAlSiO_4$ as the predominant phase with tetragonal and cubic K_2O-alumina silicates, richer in K_2O than $KAlSiO_4$, present in deeper regions of this zone.

Area c–high K content, saturated with condensed K_2CO_3.

Further analyses of "slag" material from these regions by magnetic susceptibility and XRD methods showed a high concentration of Fe_3O_4 (33 pct) between areas "a" and "b". Fe_3O_4 in area "a" was estimated at 15 pct. By comparison, anode slags measured only about 3 pct Fe_3O_4. (These estimates represent lower limits of the iron content calculated by comparing magnetic data for pure Fe_3O_4 against the slag specimens.)

The analytical data taken with the electrochemical and thermal test conditions, suggest a sequence of events which could logically account for erosion of the copper fin as indicated by Fig. 8.

First, consider the electrical conductivity of the modified slag in the region directly upstream of the copper fin. The glassy region (a) at the top is indicative of molten slag. The normal electrical conductivity of molten slag containing iron is, in this case, enhanced by the locally thickened layer noted in Fig. 9. Moreover, the deeper regions, b and c, are rich in potassium and iron ions, both contributors to current transfer. Further substantiation of ionic current transfer in this region is provided by the XRD detection of copper concentrations in regions upstream of the eroded area on the fin.

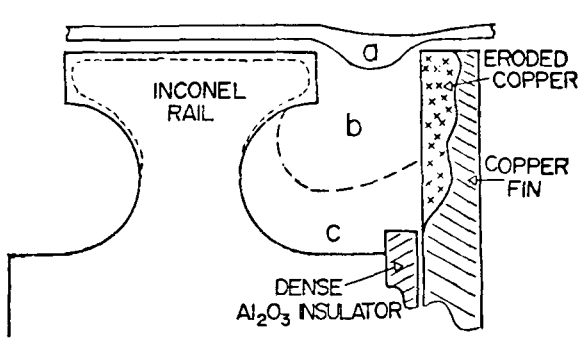

Fig. 8—Schematic diagram of cathode area between rail wall and copper fin. (*a*) Molten slag, (*b*) solidified slag, (*c*) high concentration of K and Ca.

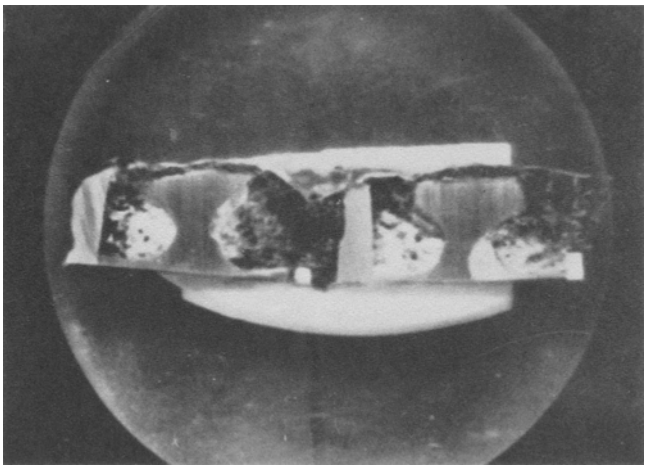

Fig. 9—Cathode rail wall cross section, magnification 2 times.

Taking all these factors into consideration, it appears that the affected region between the fin and the upstream rail constituted a miniature electrochemical cell with a copper fin anode, an Inconel cathode, and a mixed electrolytic response because the downstream copper fin is positive by approximately 20 V to the upstream Inconel cathode.

All the post-test *in situ* evidence points to electrochemical degradation in the region depicted in Fig. 8. The question begged by this observation–namely, what initiated the degradation of the Al_2O_3 between the copper fin and the Inconel rail–is not answered, however, Two mechanisms may be postulated. The first is that degradation of the Al_2O_3 cement by reaction with the seed-slag mixture was initiated chiefly through thermochemical reactions. The metamorphosed, chemically and structurally banded characteristics of the original Al_2O_3 cement suggests a predominantly thermochemical attack, abetted by the greater potassium and iron activity expected in the cathode region. As this ionic conducting structure developed, electrolytic activity was initiated, which accelerated damage to the copper fin. The other possible mechanism which must be considered is that current transport from the plasma to the cathode focused on the upstream edge of the copper fin producing severe degradation of the adjacent Al_2O_3 insulator.

The button cathodes (used in the first twenty frames) exhibited similar effects. The upstream copper lip was severely eroded. In regions closest to the downstream Inconel button, damage was restricted to the top and upstream edge. In regions further removed from the button the copper lip was completely destroyed and the upstream Al_2O_3 interelectrode insulator eroded away to depths exceeding the thickness of the Inconel button. Figure 11 shows a section through an approximately 90 deg longitudinal chord of an Inconel button. Note that the copper lip is completely gone and that the upstream insulator is eroded to a depth exceeding the thickness of the Inconel button.

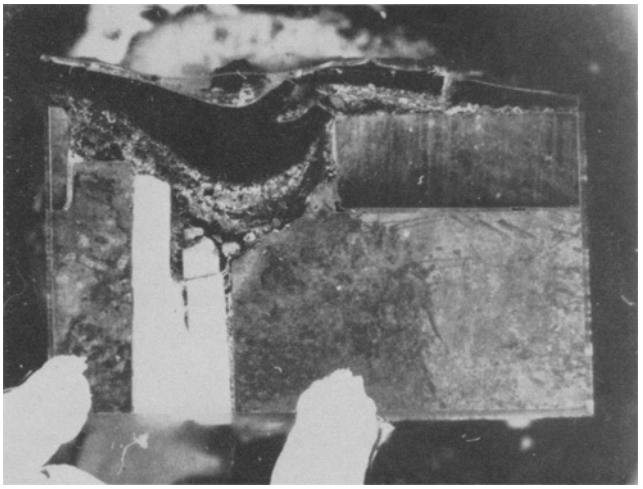

Fig. 10—Cathode button wall cross section. Rectangular dark area is Inconel button. Dark area to left of Inconel is glassy slag, magnification 4.6 times.

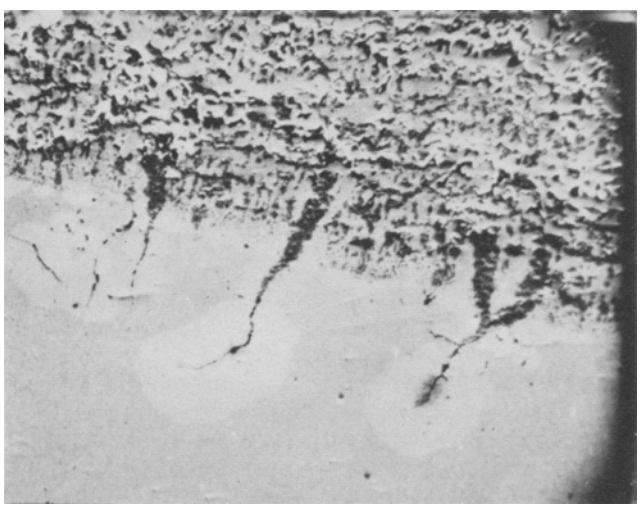

Fig. 11—SEM micrograph of damage to cathode Inconel rail, magnification 110 times.

The crescent shaped glassy region to the left of the Inconel button is considered to be indicative of rapidly solidified slag, as previously argued for the corresponding region of the rail design specimen. And, again, paralleling the situation noted in the analyses of the rail design attack, the thickened molten slag coating bridges the interelectrode gap, strongly suggesting interelectrode shorting.

The distinct chemical and structural banding observed in the rail cathode examination is not as clearly distinguishable in the button design. This is consistent with the thermal design differences between the two configurations. The button thermal design anticipates an 810 K surface temperature as against 1370 K for the rail. The thermal gradient for the button is thus much steeper than for the rail and therefore less likely to exhibit readily detectable thermally-driven segregation.

The similarities in the general distress suffered by the cathodes, noted above, suggest the existence of a severe electrochemical stress at the upstream edge of the electrode. (Note that both the copper fin, in the case of the rail, and the copper lip, in the button design, form the upstream edges of their respective electrodes.) The severe damage incurred at these selected locations of both electrode types infers locally steep current densities such as might be expected if the Faraday current preferentially sought the leading edge of the cathode. A practical materials engineering deduction is that minor differences noted in the characteristics of the damaged areas of the two designs are of much less importance than similarities in the gross condition, which, again, are believed to be associated with strong electrochemical stress concentrations. The secondary differences noted can be reasonably ascribed to heat transfer effects, *viz*, the cooler button design provided greater protection against erosion of the Inconel surface and suppressed development of the slag-seed-Al_2O_3 reaction product zones which were so clearly distinguishable in the rail specimens.

(Note: Subsequent to the above post-test analyses of the Mark VI-C 100 h test, another test was conducted in which the button cathode was reversed, *i.e.*, the copper lip was located on the *downstream* side. In this configuration, the *upstream* edges of the buttons eroded while the copper lip was relatively unaffected. This clearly shows that the $J \times B$ body force is dominant, under these test conditions, in concentrating the current at the upstream edge of the cathode.)[23]

Another, less severe form of cathode degradation was observed on the surface of the cathode rails. This is illustrated by the SEM micrograph of Fig. 11. The transgranular fissures were found on top and underside rail surfaces. SEM microscopy and X-ray mapping of a typical region clearly identified K, Ca, and Cr concentrations associated with the fissures. No explanation of the attack mechanism was deduced from the analytical observations, but the extent of attack was clearly intensified by temperature. No correlation with current concentration was evident.

(The similarity between the characteristics of this alkali metal attack and the attack exhibited in alkali metal heat transfer systems is worth noting. Both show acute sensitivity to chromium and temperature and, in addition, there are close resemblances in the form of attack.)

The AVCO Everett Research Laboratory Mark VI-C test, under slagging conditions, demonstrates several important design-material interactions.

1) On the anode wall, electrode degradation was associated with oxidation. This is circumstantially demonstrated by comparison of erosion rates of the 810 K and 1370 K designs. The latter were much more severely attacked; eroded, in fact, to an extent approaching the thermal design configuration of the buttons. Analytical evidence of oxidation as the major determinant in erosion was established by SEM examinations of the slag-Inconel interface regions. Although it cannot be stated unequivocally, there is strong evidence to suggest that anode oxidation is significantly reenforced by electrochemical activity. Comparison of erosion rates of the anode wall (higher current) with the side wall (lower current) lends direct evidence of this. It should be pointed out, furthermore, that erosion rates would logically be expected to decrease with increasing loss of surface metal. Experimental evidence of a decreasing rate is suggested by the oscillograph trace of anode wall bulk cooling water temperature.

2) The dominant erosive force on the cathode wall was, most probably, an intense electrochemical stress concentration at the leading edge of the cathode. This view is supported by gross similarities in the nature of damage sustained by the two thermal designs. The 1370 K design exhibited the same general type and localized concentration of eorsion as the 810 K design. The localized current concentration at the leading edge eroded the copper in both cases. Locally high temperatures destroyed adjacent insulator materials and probably set up secondary electrolytic forces which accelerated destruction of the copper fin.

3) Clear evidence of thermal influences are also recognizable in the cathode wall, *e.g.*, the 810 K design was less eroded than the 1370 K design. However, the 1370 K cathodes were not nearly as eroded as the 1370 K anodes, pointing again to the strong oxidation potential at the anode, as would be expected. An additional source of thermally associated damage is exhibited in the potassium and calcium attack on the 1370 K cathodes. The 810 K cathodes show no damage of this kind.

More recent tests of metal electrode designs in a Mark VI channel indicate that cold copper electrodes (770 K) are noticeably superior to higher temperature, lower thermal conductivity materials. A series of four 25 h tests showed negligible erosion of copper cathodes. Anodes, under the same conditions, eroded on the leading edge but to a much lesser extent than nickel or cobalt base alloys. Of these latter materials, TD nickel, with superior thermal conductivity, was by far the best, approaching the performance of copper. Slag accentuates erosion (oxidation) on the anode but seems to have little effect on cathode erosion. Preliminary tests of a thin platinum (0.13 mm) cladding on copper anodes were encouraging: the platinum clad was not significantly affected in 50 h, but the copper substrate was noticeably eroded (undercut) at the leading edge. A new design which extends the platinum cladding around the leading edge corner is scheduled for future test. This initial U.S. test on noble metal electrodes confirms earlier British experience.[13]

D.3. Slag Tests

Coal slag becomes a critical design element in a coal-fired MHD generator intended to operate with slag coated walls. The slag must perform two contradictory design functions: a) in the direction perpendicular to the plasma flow, it must transport current to (anode) and from (cathode) the plasma; and b) in the direction parallel to the plasma flow, it must block interelectrode current leakage. Thus, the slag acts as an electrode in the transverse direction and as an insulator in the axial direction.

The geometric and thermal design conditions which most obviously affect this dual function are: a) the ratio of the conductive path in the transverse direction (slag thickness) to the "insulative" path in the axial direction (interelectrode gap width); and b) the integrated electrical and fluid dynamic properties across the slag thickness. The effective integrated slag properties are, of course, dependent not only on the slag chemistry but, just as critically, on the steep temperature gradient across the approximately 1 mm thickness. In most designs, this gradient is steeper above the electrodes than above the interelectrode insulators.

Design Problems. As noted before, a "slagging" MHD generator anticipates slag coated channel walls. So far, U.S. development has been predicated upon slag coating of the four walls. No experimental efforts have been made to selectively coat some walls while keeping others "clean." Through proper thermal design, for example, side walls might be run in the "clean" condition while electrode walls are "slagged." Similarly, the electrode walls could be operated in either mode.

Ability to maintain a slag coating on the channel walls depends, obviously, on wall temperature and wettability. Estimates of the maximum wall temperature limit necessary to ensure slag retention vary. We may assume, however, that the maximum wall temperature at which significant slag deposits can exist is somewhat less than 1970 K. Very little of the mineral ash (from the coal combustion) or the seed will condense out above this temperature. At wall temperatures between approximately 1470 and 1970 K the slag layer will usually be entirely liquid. Retention of slag at the upper end of this range may be difficult, however, because of excessive fluidity. A critical viscosity exists below which the slag will flow as a true liquid, with negligible integrated shear strength. In this range, the coating will be quite thin, assuming slag is retained at all. Surface wettability characteristics are clearly of major design influence in this range.

At wall temperatures below about 1470 K a solidified layer of slag can be expected at the slag-wall interface. Lowering the temperature further thickens the solidified layer. A wall temperature of 820 K would be expected to sustain a slag coating thickness of approximately 1.5 mm. It should be pointed out that thermal losses incurred in reducing the wall temperature of a "slagging" wall generator are negligible since the slag surface temperature is relatively insensitive to the wall temperature.

A number of critical variables must be considered in evaluating slag conditions in relation to design performance. Coal characteristics and treatment, combustion conditions, and mass flow all affect chemical and physical characteristics of the slag deposits on the channel walls. Dynamic tests are particularly important, as suggested by the test experience reviewed in the following section.

Dynamic Slagging Rig Tests. Investigators at Stanford University are studying slag deposition characteristics and current transport through slag layers.[24] The test apparatus comprises a fuel and oxidant flow system, combustor, slag deposition test section, an electrode module, a diagnostic section, and suitable exhaust components. Independent control of oxidant, fuel, coal or ash, and nitrogen allows simulation of a wide range of ash carry-over into the test section. The slag deposition test section has a constant 3.8 cm × 7.6 cm cross section and is 45.7 cm long. One side wall and the top wall are made of copper, transversely grooved and cooled to a surface temperature of 405 K. The remaining side wall is smooth magnesia with a surface temperature in the 1700 to 1900 K range. The bottom wall is made up of six grooved-type 304 SS

slabs designed to operate at ~1000 K. The transverse grooves in the stainless and copper surfaces are filled with castable ceramic to facilitate slag wetting.

An electrode module is attached to the downstream end of the deposition section. The electrodes, 1.3 cm long by 3.8 cm wide, are cooled by water or nitrogen to provide a wide range of test temperatures. Tests have been run with mild steel and stainless steel (type 304) electrodes. Platinum voltage probes on the magnesia side walls (where slag layers are thin) are used to measure potential drops across the gas path.

The two series of experiments were carried out under an applied electric field. Both used Rosebud coal and both were conducted with gas temperatures of around 2700 K. Ash mass fraction and combustor plug flow residence times differed: in the first test, ash flow and residence time were 0.84 pct and 18.5 ms, respectively, while in the second test they were 0.46 pct and 39.3 ms. In the first series of tests, the electrode temperature was maintained at 555 K ("cold electrode") and, in the second, between 1000 and 1400 K ("warm electrode"). The cathode side only was observed in the first series with average current densities up to 0.6 A/cm^2. Both anode and cathode surfaces were observed in the second series at current densities up to 3.7 A/cm^2.

These tests provide an opportunity to examine, under a given set of conditions, the influence of electrode polarity and electrode surface temperature on electrical conduction characteristics. This is possible because slagging conditions were reasonably constant, except, of course, for such chemical and physical differences as would be induced by electrochemical influences.

Considering first the "cold" (550 K) cathode tests, bright "hot spots" were observed at the slag surface for all current densities, *e.g.*, 0.04 to 0.66 A/cm^2. The hot spots typically formed on or near the most completely developed (flowing region) of the slag layer. Based upon the measured diameter of a typical large quasi-steady hot-spot which formed on the leading edge of an electrode, localized current concentrations were estimated to be approximately 16 A/cm^2. Here, the Stanford scientists' verbatim comments are illuminating, to wit:

"The joule dissipation from this concentrated discharge elevates the slag surface temperature locally which increases the slag fluidity. A region of hot, fluid slag emanating down stream from the hot-spot can be observed. During post-test examination of this electrode, a large eroded area was observed in the same location as this large hot-spot. A third form of hot spot . . . (occurs when) a "large" hot-spot "burns" a hole of about 2 mm diam through the slag layer. The bright periphery of the hole implies that the electric discharge is through the slag at the boundary of the hole. This hole closed up and reformed several times. At one point, the upstream slag flow was temporarily sufficient to quench this hot-spot and the above sequence repeated itself with the initial formation of several random smaller hot-spots developing into one larger quasisteady spot."[24]

The warm electrode tests (1000 to 1400 K) disclosed three distinct current discharge modes which could be correlated with current density and electrode temperature conditions. These may be described as: a) a stable diffuse mode; b) a quasi-stable hot-spot mode; and c) an unstable slag layer mode. In the stable diffuse mode, the passage of current through the slag has no visible effect on the slag surface. The quasistable mode is characterized by the emergence of brighter areas (hot spots), particularly at leading edges. The hot spots appear to interact with the flowing slag and are mobile, sometimes moving downstream. The slag layer flow is sufficient, however, to prevent destruction of the slag coating. The unstable slag layer mode is marked by the formation of intense hot spots which destroy the slag layer locally and propagate down the slag-void boundary producing further disintegration of the slag coating.

Transition from the stable mode to the quasistable condition and then to the unstable was influenced strikingly by current density and electrode temperature. For the anode, the limited data available (ten points) suggest that the stable mode is promoted by either decreasing current densities or increasing temperatures (at least within limits represented by the test conditions, namely CDs between 0.2 and 2.5 A/cm^2 and electrode temperatures between 1000 and 1400 K). Unstable discharge was observed in three of the four anode tests in which temperature conditions fell below 1240 K when current densities exceeded 1.0 A/cm^2.

Cathode behavior showed considerably greater sensitivity to current densities, regardless of temperature, than the anode. Five of six tests made with current densities above about 1.8 A/cm^2 displayed quasistable discharge behavior even at temperatures up to 1400 K. The sixth exhibited unstable characteristics at a cathode temperature of about 1000 K. Two tests below 1.8 A/cm^2 showed stable discharge but these were run at 1400 K. By comparison, a "cold" (550 K) cathode test displayed a constricted, hot-spot discharge at a current density below 1.8 A/cm^2.

Detailed analyses of these data by Stanford scientists suggests that stability in the anode region may be correlated on theoretical grounds with wall temperature and with published slag properties.[25] Further, cathode stability is associated both with wall temperature and thermionic emission limitations. An effective work function of 2.9 eV was postulated for the slag surface.

A second slag program which deserves mention is being conducted by Stickler and his associates at the AVCO Everett Research Laboratory, Inc.[26] There, investigations have been directed more toward the quantitative delineation of slag transport, slag layer development, and fluid dynamic behavior in the absence of electric field effects. Variables studied include velocity, wall temperature, wall material, slag mass flow, and seed flow.

The University of Tennessee Space Institute (UTSI), where coal-fired, slagging MHD generator development was pioneered, is continuing studies of slagging phenomena.[27] Test work at MIT[28] and Westinghouse Electric Corporation[29] is contributing directly to the evaluation of electrode module designs under simulated generator thermal and electrochemical design stresses.

The foregoing review of "slagging" tests illuminates some of the complex slag-design interactions which are unique to MHD. Materials engineering responsibility is primarily concerned here with quantifying the combined effects of slag thermal, chemical, physical, and electrical properties on design performance. The importance of simulating the design environment in testing is obvious.

E. SUMMARY

This review has emphasized especially the unique combination of fluid-dynamic, electrodynamic, electrochemical, and thermal conditions which MHD generator materials endure. The following observations, based upon the generator test results reported here, appear to be of particular significance to design material selection.

a) Slag coated metal (Inconel) anodes are susceptible to localized oxidation at the leading edge. Damage was much more severe at 1370 K (design surface temperature) than at 540°C, indicating a strong thermal influence. Current concentration and possibly microarcing at the leading edge is indicated. Preliminary tests of "cold" copper anodes under similar MHD conditions, *i.e.*, 0.8 A/cm^2 and 1500 V/m, show significantly less erosion in 50 h than Inconel under the same conditions. This confirms University of Tennessee experience with "cold" copper electrodes. In other recent tests, thin platinum claddings were not significantly affected in 50 h, although the copper substrate showed some erosion at the abutting edge on the up-stream face.

b) Slag coated Inconel cathodes at 1370 or 810 K were damaged by current concentrations at the leading edge, resulting in localized destruction of the interelectrode insulation. General erosion of the 810 K, cathode was considerably less than the 1370 K design, indicating a significant thermal influence. Also, potassium attack was observed on the 1370 K design but not on the 810 K design. "Cold" Cu and 60W-40Cu cathodes showed no visible damage in 50 h under similar test conditions.

c) Interelectrode insulation damage on metal electrode walls is mitigated by high thermal diffusivity electrode-insulator design. Copper electrodes at 770 K combined with boron nitride insulators were superior in this regard.

d) In higher temperature ceramic electrode systems (walls > 1970 K), interelectrode insulators display considerable potassium penetration, particularly on the cathode side. Porosity, either in the insulator itself or in adjacent castable ceramic joints, is believed to promote this potassium attack. Subsurface regions, where K vapor condenses, shows greatest K concentrations.

e) High temperature ceramic electrodes may display phase instabilities. This applies particularly to ZrO_2-CeO_2 materials, in which CeO_2 volatilization is experienced.

It should be noted that the metal electrode tests described in this review more closely reflect true power generation duty requirements than do the ceramic wall tests. Hall voltage differences are particularly worth noting: the metal electrode tests were made with Hall voltages exceeding 1500 V/m while the USSR "hot wall" tests were in the 500 to 600 V/m range. Heat fluxes were also more realistic, *e.g.* up to 300 W/cm^2 as compared to a maximum of 30 W/cm^2 in the U-02 tests.

These tests exemplify the broad range of design conditions which are presently being considered in open-cycle MHD generator development. In a simplistic view, the high temperature, ceramic material approach minimizes electrodynamic (arcing) stresses but intensifies chemical and electrochemical activity. Chemical reaction of the seed with insulators, high temperature structural instabilities, and solid state diffusion are all potential threats to durability. Another potential source of trouble is the interface between the metal lead-out and the ceramic electrode. Thermal design requires a delicate balance between conductivity of the ceramic and thermal resistance of the metal. Recent tests in the U-02 have, however, provided some encouragement in solving these problems. Highly densified MgO exhibited much improved resistance to potassium attack. Furthermore, several spinel type electrodes have exhibited good thermal stability combined with electronic conductance to temperatures as low as 770 K. These include 0.75 $MgAl_2O_4$-0.25 Fe_3O_4 (Ref. 30) and 0.75 $FeAl_2O_4$-25 Fe_3O_4.[28] Lanthanum chromite La(Mg)CrO_3 also possessed desirable properties and has performed well in preliminary tests.[31]

Contrasted with the high temperature ceramic design, the lower temperature metallic electrode system, while minimizing gross thermally-dependent chemical and electrochemical attack, must deal with more intense electrodynamic stresses. Experimental evidence strongly suggests that damage from this source can be minimized by raising the thermal diffusivity of the system. Colder Inconel anodes (810 K) showed much less oxidation than warm (1370 K) anodes. Similar improvement was observed in Inconel cathode erosion (presumably by K attack) and insulator damage. Additional evidence is available in the improved performance obtained with cold copper electrodes. Evidently, the localized thermal spike produced by an arc (or current concentration) is effectively quenched in a high thermal diffusivity system. This points to the importance of high thermal conductivity insulators. The arcs, or current concentrations, typically appear at electrode edges, adjacent to the insulator. Rapid diffusion of these thermal effects depends strongly on both insulator and electrode temperatures and conductivities. Boron nitride showed considerable promise for this purpose. Even higher conductivity, *e.g.* BeO, could be expected to further dissipate arc heating at electrode edges. Another major advantage of such a high thermal conductance insulator is that the temperature of the slag at the insulator surface would be lowered. This would increase electrical resistivity across the interelectrode gap.

In a greatly simplified manner, then, engineering design selection between "hot" ceramic and "cold" metallic electrodes may translate to a choice between: a) high temperature electrochemical problems involving a relatively narrow group of electronically conducting ceramic electrodes and dense, chemically inert, structurally stable ceramic insulators; and b) mitigation of the destructive effect of arc discharge through rapid heat dissipation by a highly thermally-conductive and structurally inert electrode-insulator combination.

ACKNOWLEDGMENTS

For critical discussions necessary to the preparation of this review paper, the author is grateful to Dr. Albert Solbes and Mr. Stanley Petty of the AVCO-Everett Research Laboratory, Inc.; Mr. William R. Hosler of the National Bureau of Standards; Dr. J. K.

Koester of Stanford University; and Dr. Enrico Levi of the Division of MHD, Energy Research and Development Administration. Gratitude is expressed also to Miss Jean Grimes and Miss Cathy Campbell for excellent support in typing and editing the manuscript. Finally, the authors wishes to thank Dr. W. D. Jackson for encouraging the preparation of this paper.

REFERENCES

1. G. R. Seikel *et al*: "Proceedings of the Fifteenth Symposium on the Engineering Aspects of Magnetohydrodynamics," Philadelphia, Pa., May 24-26, 1976. (Available from Dr. John Fox, Department of Mechanical Engineering, University of Mississippi, University, Miss. 38677.)
2. W. D. Jackson: "AIAA Ninth Fluid and Plasma Dynamics Conference," AIAA Paper No. 76-309, San Diego, Calif., July 14-16, 1976.
3. Electric Power Research Report No. EPRI SR-12.
4. *Open Cycle MHD Power Generation*: J. B. Heywood and G. J. Womack, eds., pp. 395-465, Pergamon Press, Oxford, England, 1969.
5. A. Solbes and A. Lowenstein: "Proceedings of the Fifteenth Symposium on the Engineering Aspects of Magnetohydrodynamics," Philadelphia, Pa., May 24-26, 1976.
6. D. A. Oliver: *Ibid.*
7. E. R. Plante, C. D. Olsen, and T. Negas: "Sixth International Conference on MHD Electrical Power Generation," vol. II, p. 211, Washington, D.C., 1975. Available from National Technical Information Service (NTSI), U.S. Department of Commerce, 5285 Port Royal Road, Springfield, Va. 22161.
8. H. P. R. Frederikse and W. R. Hosler: "Proceedings of the Fourteenth Symposium Engineering Aspects of Magnetohydrodynamics," University of Tennessee, Space Institute, 1974.
9. C. K. Peterson and R. W. Ure, Jr.: "Proceedings of the Fifteenth Symposium on Engineering Aspects of Magnetohydrodynamics," Philadelphia, Pa., 1976.
10. J. L. Bates: "Sixth International Conference on MHD Electrical Power Generation," vol. II, p. 163, 1975.
11. M. Bogdanska, W. S. Brzozowski, J. Charuba, K. Dabrowski, M. Plata, and M. Zielinski: "Sixth International Conference on MHD Power Generation," vol. II, p. 9, 1975.
12. T. O. Mason, W. T. Petuskey, W. W.Lang, J. W. Halloran, F. Yen, T. M. Pollack, J. F. Elliot, and H. K. Bowen: "Proceedings of the Sixth International Conference on Magnetohydrodynamic Electrical Power Generation," vol. II, Washington, D.C., 1975.
13. *Open Cycle MHD Power Generation*: J. B. Heywood and G. J. Womack, eds., pp. 499-605, Pergamon Press, Oxford, England, 1969.
14. G. Rudins: R-1656-ARPA, ARPA Order No. 189-1, 6610 Technology Assessment Office, The Rand Corporation, Santa Monica, Calif., 1974.
15. W. R. Hosler and H. P. R. Frederikse: "Sixth International Conference on MHD Electrical Power Generation," Washington, D.C., 1975.
16. J. C. L. Wu, J. B. Dicks, K. E. Templemeyer, L. W. Crawford, I. W. Muelhauser, and G. Rajagopal: "Sixth International Conference on MHD Electrical Power Generation," vol. I, p. 199, 1975.
17. S. W. Petty, A. Solbes, G. Enos, and J. P. Morenski: "Joint US-USSR Colloquium on MHD Power Generation," Moscow, USSR, 1976, in publication.
18. J. A. Dilmore, J. Lempert, A. B. Turner, S. Way, and W. E. Young: "Proceedings of the Fifteenth Symposium on Engineering Aspects of Magnetohydrodynamics," Philadelphia, Pa., 1976.
19. G. Rudins: Defense Advanced Research Projects Agency Report R-1404-ARPA, ARPA Order No.:189-1, pp. 32-34, January, 1974.
20. W. D. Jackson, S. J. Schneider, W. E. Young, A. E. Sheindlin, G. P. Telegin, and D. K. Burenkov: "Proceedings of the Fifteenth Symposium on Engineering Aspects of Magnetohydrodynamics," Philadelphia, Pa., 1976.
21. S. Petty, A. Solbes, G. Enos, and A. Dunton: "Proceedings of the Fifteenth Symposium on Engineering Aspects of Magnetohydrodynamics," Philadelphia, Pa., 1976.
22. W. R. Hosler, T. Negas, and S. W. Petty: "Proceedings of the Fifteenth Symposium on Engineering Aspects of Magnetohydrodynamics," Philadelphia, Pa., 1976.
23. Unpublished data, AVCO Everett Research Laboratories, 1977.
24. J. K. Koester, M. E. Eustis, and J. K. Rodgers: "Proceedings of the Fifteenth Symposium on Engineering Aspects of Magnetohydrodynamics," Philadelphia, Pa., 1976.
25. J. L. Bates: NSF-RANN Grant G1-44100 Report, Batelle Pacific Northwest Laboratories, August, 1975.
26. D. B. Stickler and R. DeSaro: "Proceedings of the Fifteenth Symposium on Engineering Aspects of Magnetohydrodynamics," Philadelphia, Pa., 1976.
27. L. W. Crawford:*et al*: "Proceedings of the Fifteenth Symposium on Engineering Aspects of Magnetohydrodynamics," Philadelphia, Pa., 1976.
28. R. L. Pober, J. L. Nash-Weber, M. Yoshimura, and H. K. Bowen: *Ibid.*
29. B. R. Rossing, J. A. Delmore, H. D. Smith, and W. E. Young: *Ibid.*
30. H. P. R. Frederikse, A. J. Armstrong, and W. R. Hosler: *Ibid.*
31. Unpublished data, Westinghouse Electric Corporation, 1977.